RAA 2014 Vol. **14** No. **2**, 144–158 doi: 10.1088/1674–4527/14/2/003
http://www.raa-journal.org *http://www.iop.org/journals/raa*

Research in Astronomy and Astrophysics

Revisiting the dichotomy of early-type galaxies *

Yan-Qin He[1,2,3], Cai-Na Hao[3] and Xiao-Yang Xia[3]

[1] University of Chinese Academy of Sciences, Beijing 100049, China
[2] National Astronomical Observatories, Chinese Academy of Sciences, Beijing 100012, China
[3] Tianjin Astrophysics Center, Tianjin Normal University, Tianjin 300387, China; *cainahao@gmail.com*

Received 2013 September 6; accepted 2013 September 18

Abstract We study the relationship between isophotal shapes, central light profiles and kinematic properties of early-type galaxies (ETGs) based on a compiled sample of 184 ETGs. These sample galaxies are included in Data Release 8 of the Sloan Digital Sky Survey and have central light profiles and kinematic properties available from the literature, which were compiled from observations by the *Hubble Space Telescope* and the ATLAS^{3D} integral-field spectrograph, respectively. We find that there is only a weak correlation between the isophotal shape (a_4/a) and the central light profile (within $1\,\mathrm{kpc}$) of ETGs. About two-fifths of "core" galaxies have disky isophotes, and one-third of "power-law" galaxies are boxy. Our statistical results also show that there are weak correlations between galaxy luminosity and dynamical mass with a_4/a, but such correlations are tighter with a central light profile. Moreover, no clear link has been found between the isophotal shape and the Sérsic index. Comparisons show that there are similar correlations between a_4/a and ellipticity, and between a_4/a and specific angular momentum $\lambda_{R_\mathrm{e}/2}$ for "power-law" ETGs, but there are no such correlations for "core" ETGs. Therefore, we speculate that the bimodal classifications of ETGs are not as simple as previously thought, though we also find that the disky ETGs with highest a_4/a are more elongated and fast rotators.

Key words: galaxies: elliptical and lenticular, cD — galaxies: kinematics and dynamics — galaxies: photometry — galaxies: structure

1 INTRODUCTION

The formation or assembly history of early-type galaxies (hereafter ETGs) has been a hot topic in the field of galaxy formation and evolution. Since the formation history of ETGs can be imprinted on their photometric and kinematical properties, extensive efforts have been made to explore these properties utilizing both imaging and spectroscopic observations. Subsequently, significant progress has been made. In particular, dichotomies in isophotal shapes, nuclear light profiles and kinematics were found. In most cases, isophotal shapes were not perfect ellipses. Fourier analyses of the deviations from ellipses showed that the most significant non-zero component is the coefficient of the fourth cosine term (i.e., a_4/a; see Lauer 1985; Bender et al. 1988, 1989; Hao et al. 2006; Kormendy

* Supported by the National Natural Science Foundation of China.

et al. 2009). The sign of a_4/a was used to divide ETGs into two classes: boxy ($a_4/a < 0$) and disky ($a_4/a > 0$) (Bender et al. 1988; Faber et al. 1997). Interestingly, some other properties have also shown that boxy and disky ETGs are two different populations. Boxy ETGs tend to be bright, have strong radio and X-ray emission, and rotate slowly while disky ETGs are faint, radio-quiet, have no hot gaseous halos that emit X-rays and show regular rotation patterns.

Similarly, a dichotomy was also found in the central properties of ETGs. Based on high resolution images obtained by the *Hubble Space Telescope (HST)*, it was found that the central surface brightness profiles of ETGs could be fitted by a "Nuker Law" with the form $\Sigma(\mathrm{r}) \sim \mathrm{r}^{-\gamma}$ (Crane et al. 1993; Ferrarese et al. 1994; Lauer et al. 1995). ETGs with steep inner cusps ($\gamma > 0.5$) are classified as "power-law" galaxies, while ETGs with shallow inner profiles ($\gamma < 0.3$) are called "core" galaxies (Lauer et al. 1995; Faber et al. 1997). In a more recent study, Lauer et al. (2007b) introduced γ' as an indicator of the bimodal classification, which is the local slope at the limit of angular resolution for the *HST*, instead of γ that is the slope of the inner cusp as $r \to 0$. ETGs with $\gamma' > 0.5$ are called "power-law" galaxies; "core" galaxies are those with $\gamma' < 0.3$, and the rest, i.e. ETGs with $0.3 < \gamma' < 0.5$, are classified as "intermediate" type. The inner slope of the central profile of ETGs is correlated with their global physical properties such as luminosity, rotation velocity and isophotal shape (Faber et al. 1997; Lauer et al. 2007b).

The kinematic properties of ETGs were usually described by a ratio of the rotational velocity to the velocity dispersion (v/σ). Recently, the SAURON survey proposed a new tracer of the kinematic properties of ETGs, which is the specific angular momentum λ_R (see Sect. 3), to divide ETGs into fast and slow rotators (e.g. de Zeeuw et al. 2002; Emsellem et al. 2007). As an extension of the SAURON survey, the ATLAS$^{3\mathrm{D}}$ team conducted a multi-wavelength survey of a carefully selected volume-limited sample of ETGs with 260 objects using the SAURON integral-field spectrograph. Based on these observations, the ATLAS$^{3\mathrm{D}}$ team quantitatively classified ETGs into fast and slow rotators by using $\lambda_R = 0.1$ (e.g. Krajnović et al. 2011). Fast rotators have regular stellar rotation with alignments between the photometric and kinematic axes, low luminosity and large ellipticity, while slow rotators show little or no rotation, and tend to be more massive and rather round (e.g. Cappellari et al. 2007; Emsellem et al. 2007, 2011).

Given that dichotomies have been found in isophotal shapes, nuclear light profiles and kinematics, it is interesting to investigate relations between these properties and with other galactic properties. Several studies have focused on such issues but reached conflicting conclusions. Krajnović et al. (2013) compared the nuclear light profiles and large scale kinematics of 135 ETGs, and concluded that there is no evidence for a bimodal distribution in the nuclear slope. Emsellem et al. (2011) also pointed out that the a_4/a parameter appears not to be directly related to the kinematic properties of ETGs. In short, the ATLAS$^{3\mathrm{D}}$ team argued against the dichotomy of ETGs based on their isophotal shape (a_4/a) and nuclear light profile. However, Lauer (2012) investigated the relation between the kinematics and central structures based on a sample of ETGs with 63 objects and found that they are well correlated if a criterion of $\lambda_{R_\mathrm{e}/2} = 0.25$ (see Sect. 3) is used to separate fast from slow rotators. The correlation shows that slow rotating ETGs usually have cores, but "power-law" galaxies tend to rotate rapidly.

From a theoretical point-of-view, simulations of galaxy formation indicate that the bimodality of isophotal shapes and central profiles of ETGs are correlated with galaxy merger histories, but such relations are complicated. The dissipationless simulations by Naab & Burkert (2003) and Naab & Trujillo (2006) showed that the equal-mass mergers of two disk galaxies tend to produce boxy ETGs, but unequal-mass mergers lead to disky ETGs. However, Khochfar & Burkert (2005) found that the isophotal shapes of merger remnants not only depend on the mass ratio of the last major merger, but also on the morphology of their progenitors and the subsequent gas infall. Using hydrodynamical simulations, Hopkins et al. (2009a,b) concluded that "power-law" ETGs are formed by dissipational mergers (wet-mergers) in the sense that cases described by the inner extra light/outer profile are formed in a compact central starburst/outer violent relaxation, whereas "core" galaxies are formed by

dry-mergers through subsequent merging of gas-poor ellipticals. During the process of dry-merging, the center becomes dense and compact because the merging binary black holes scatter the inner stars.

Therefore, there is still a debate on the dichotomy of ETGs and their formation history from both observational and theoretical perspectives. In this work, we re-investigate the correlations among isophotal shapes, central light profiles and kinematic properties of ETGs based on a large compiled sample of 184 ETGs observed by both *HST* and the Sloan Digital Sky Survey Data Release 8 (SDSS DR8).

The paper is structured as follows. In Section 2 we describe the sample used for this work. Then we outline the data reduction in Section 3. We present the main results in Section 4 and finish with a summary in Section 5. We adopt a Hubble constant of $\mathrm{H}_0 = 70\,\mathrm{km\,s^{-1}Mpc^{-1}}$, a cosmology with matter density parameter $\Omega_m = 0.3$ and a cosmological constant of $\Omega_\Lambda = 0.7$.

2 SAMPLE

To explore the relations between isophotal shapes, central light profiles and kinematics of ETGs, we need a sample of ETGs with these properties being compiled. As mentioned in the introduction, in the literature there are large samples of ETGs that have been observed with the *HST* and their central light profiles have been scrutinized. However, these observations only cover the central parts of the ETGs because of the small field of view of *HST*. Therefore SDSS images will be used to measure the global properties of ETGs instead.

Our sample of ETGs is compiled from three sources. The first is from the cross-correlation of the SDSS DR8 photometric catalog with 219 ETGs collected by Lauer et al. (2007b). The sample of galaxies in Lauer et al. (2007b) was observed by *HST*, WFPC2 ($36.5'' \times 36.5''$, $0.046''$/pixel, Rest et al. 2001; Laine et al. 2003; Lauer et al. 2005), WFPC1 ($66'' \times 66''$, $0.043''$/pixel, Lauer et al. 1995; Faber et al. 1997) and NICMOS ($19.2'' \times 19.2''$, $0.076''$/pixel, Quillen et al. 2000; Ravindranath et al. 2001). It encompasses 117 "core" galaxies, 89 "power-law" galaxies and 13 "intermediate" galaxies. The cross-correlation of these 219 ETGs with the SDSS DR8 leads to 111 ETGs, in which there are 54 "core" galaxies, 54 "power-law" galaxies and 3 "intermediate" galaxies, respectively. The second is taken from Krajnović et al. (2013) with 135 ATLAS$^{3\mathrm{D}}$ galaxies available in the *HST* archive. However, 61 out of 135 ETGs have been included in Lauer et al. (2007b). A cross-correlation of the remaining 74 objects with the SDSS DR8 photometric catalog leaves us with 52 ETGs, consisting of 3 "core" galaxies, 37 "power-law" galaxies and 12 "intermediate" galaxies. The third is from the cross-correlation of the SDSS DR8 photometric catalog with the sample of 23 ETGs studied by Hyde et al. (2008), which were observed with the Advanced Camera for Surveys (ACS) on *HST* and the velocity dispersions are larger than 350 km s^{-1}. From this, 21 ETGs were selected, including 6 "core" galaxies, 9 "power-law" galaxies and 6 "intermediate" galaxies. In total, we construct a sample of ETGs with 184 galaxies, which consist of 63 "core" galaxies, 100 "power-law" galaxies and 21 "intermediate" galaxies. The redshifts of 111 ETGs from Lauer et al. (2007b) and 52 ETGs from Krajnović et al. (2013) are less than 0.04, while the 21 ETGs from Hyde et al. (2008) are in the range $0.1 < z < 0.3$. All ETGs are in the luminosity range $-24 < M_V < -15$.

3 DATA REDUCTION AND PARAMETER ESTIMATION

We obtained the corrected frame fpC-images in the r-band for our sample ETGs directly from the SDSS DR8 Data Archive Server. For each frame (2048×1489 pixels), reductions including bias subtraction, flat-fielding, pixel defects and cosmic ray correction have been performed by the SDSS photometric pipeline (PHOTO, Lupton et al. 2001).

The background subtraction process was similar to that of Liu et al. (2008) and He et al. (2013), which has been successfully applied to the brightest ETGs. In the following, we briefly outline this approach. First, SExtractor (Bertin & Arnouts 1996) has been used to generate an image with only background that has all detected objects flagged out. Then a median filter with 51×51 pixels is used

to convolve this image of the background. After the median filtering is performed, second-order Legendre polynomials are fitted to rows and columns separately by using the IRAF/NFIT1D task. Finally, we obtain a model of the sky background by using a circular Gaussian filter with $\sigma = 9$ pixels to smooth the fitted frame. This model of the sky background is then subtracted from the original SDSS corrected frame. After sky background subtraction is done, the frame is trimmed to 501×501 pixels with the target galaxy centered and other objects masked out using SExtractor. In the following, isophotal photometry will be performed on this final trimmed frame.

The IRAF/ELLIPSE task is used to perform the surface photometry. Given some initial values for the geometric center of the galaxy, ellipticity, length of the semimajor axis and position angle, the task fits the isophotes by a series of elliptical annuli from the center to the outskirts, with a logarithmic step of 0.1 along the semimajor axis. The output of IRAF/ELLIPSE includes the mean isophotal intensity, the position angle, the ellipticity ϵ for each annulus and deviations from perfect ellipses represented by the fourth harmonic amplitude of Fourier analyses as a function of the semi-major axis. We derive the characteristic parameters a_4/a and ellipticity ϵ by weighting them with the flux within the elliptical annulus over a region of twice the full width at half maximum of seeing to generate the effective radius $R_{\rm e}$.

Apart from a_4/a and ϵ, several other galactic properties including the Sérsic index, luminosity and dynamical mass are calculated. The Sérsic index n and effective radius $R_{\rm e}$ were obtained by fitting a Sérsic model that is convolved with the point spread function (Sersic 1968) to the r-band sky-subtracted images using the algorithm GALFIT (Peng et al. 2002). The absolute magnitude is derived by $M = m - 5\log(D_{\rm L}/10\,{\rm pc}) - A - k$, where the apparent Petrosian magnitude m and the extinction A are taken from the SDSS DR8 photometric catalog, $D_{\rm L}$ is the luminosity distance and the k-correction k is derived using the KCORRECT algorithm of Blanton & Roweis (2007). In order to transform the SDSS photometric data to the standard *UBVRI* Vega magnitude system, a formula from Smith et al. (2002) has been used to calculate the absolute magnitude of the galaxy in the V-band. We derive the dynamical mass of sample ETGs based on the formula $M_{\rm dyn} \approx \sigma^2 R_{\rm e}/G$, where σ is the corrected velocity dispersion at effective radius $R_{\rm e}$ following von der Linden et al. (2007). In our sample of ETGs, the velocity dispersions σ are available for 136 objects, including the central velocity dispersions for 101 ETGs obtained from Lauer et al. (2007a) and the velocity dispersions of 35 other ETGs from the SDSS DR8 spectroscopic catalog.

To compare with the central surface brightness profile and kinematic properties, the characteristic parameters γ', r_γ and $\lambda_{R_{\rm e}/2}$ were taken from the literature (Lauer et al. 2007a,b; Hyde et al. 2008; Cappellari et al. 2011; Krajnović et al. 2013). We briefly describe the way they were derived. The central surface brightness profile is fitted by a "Nuker Law" with the following form

$$I(r) = 2^{(\beta-\gamma)/\alpha} I_b \left(\frac{r_b}{r}\right)^{\gamma} \left[1 + \left(\frac{r}{r_b}\right)^{\alpha}\right]^{(\gamma-\beta)/\alpha}, \quad (1)$$

where the break radius r_b is the point of maximum curvature in log-log coordinates, I_b is the surface brightness at r_b, $-\beta$ is the asymptotic outer slope, α is the sharpness of the break, and γ is the slope of the inner cusp as $r \to 0$ and is distinct from γ', which is the local slope evaluated at the *HST* angular resolution limit r_0, where

$$\gamma' \equiv -\frac{d\ \log\ I}{d\ \log\ r}\bigg|_{r=r_0} = -\frac{\gamma + \beta(r_0/r_b)^{\alpha}}{1 + (r_0/r_b)^{\alpha}}. \quad (2)$$

As described in the introduction, the ETGs are classified into disky ($a_4/a > 0$) and boxy ($a_4/a < 0$) galaxies by their isophotal shapes, and they are also divided into "core" ($\gamma' < 0.3$), "power-law" ($\gamma' > 0.5$) and "intermediate" ($0.3 < \gamma' < 0.5$) galaxies according to their central

light profiles. For "core" galaxies, the physical scale of the core is characterized by the "cusp radius," r_γ, which is a radius at which γ' equals 0.5. Specifically, r_γ is given by

$$r_\gamma \equiv r_b \left(\frac{0.5-\gamma}{\beta-0.5}\right)^{1/\alpha}. \tag{3}$$

The specific angular momentum parameter λ_R is used as a discriminator of fast and slow rotators, where λ_R is defined as

$$\lambda_R = \frac{\sum_{n=1}^{N} F_n R_n |V_n|}{\sum_{n=1}^{N} F_n R_n \sqrt{V_n^2+\sigma_n^2}}. \tag{4}$$

Here F_n is the flux, R_n is the circular radius from the center of the galaxy, and V_n and σ_n are velocity and velocity dispersion inside the nth spatial radial bin. In particular, $\lambda_{R_e/2}$ is the λ_R measured within half of the effective radius R_e.

We list all these parameters for "core," "power-law" and "intermediate" galaxies in Tables 1, 2 and 3, respectively.

Table 1 "Core" Galaxy Parameters

No.	Galaxy	γ'	r_γ	R_e	σ	a_4/a	ε	M_V	$\log\frac{M_{dyn}}{M_\odot}$	n	$\lambda_{R_e/2}$
			log(pc)	log(pc)	(km s^{-1})	(10^{-2})		(mag)			
(1)	(2)	(3)	(4)	(5)	(6)	(7)	(8)	(9)	(10)	(11)	(12)
1	IC 0613	0.25[b]	2.05[a]	3.97	262[a]	0.125±0.010	0.084±0.002	−22.27	11.17	5.26	–
2	IC 0664	0.12[b]	2.07[a]	4.84	336[a]	−0.286±0.014	0.229±0.002	−22.86	12.26	8.87	–
3	IC 0712	0.17[b]	2.69[a]	4.75	345[a]	0.132±0.006	0.188±0.001	−23.29	12.19	7.79	–
4	IC 1565	−0.03[b]	1.65[a]	3.75	303[a]	−0.008±0.074	0.046±0.002	−22.99	11.08	14.59	–
5	IC 1695	0.23[b]	2.36[a]	4.74	364[a]	0.049±0.097	0.234±0.004	−23.90	12.23	8.22	–
6	IC 1733	−0.01[b]	2.68[a]	4.59	301[a]	0.433±0.088	0.126±0.002	−23.43	11.91	4.87	–
7	J010803.2+151333.6	0.23[d]	–	4.22	304[e]	−0.026±0.054	0.170±0.007	−23.19	11.55	3.28	–
8	J083445.2+355142.0	0.06[d]	–	4.60	366[e]	0.067±0.088	0.175±0.007	−23.71	12.09	4.96	–
9	J124609.4+515021.6	0.21[d]	–	4.38	387[e]	0.509±0.090	0.097±0.012	−23.85	11.92	3.99	–
10	J141341.4+033104.3	−0.09[d]	–	4.77	364[e]	−0.119±0.112	0.162±0.012	−23.42	12.26	1.89	–
11	J171328.4+274336.6	0.04[d]	–	4.49	414[e]	0.865±0.093	0.171±0.013	−24.17	12.09	5.61	–
12	J211019.2+095047.1	0.17[d]	–	4.25	371[e]	−0.981±0.053	0.144±0.006	−23.78	11.76	2.00	–
13	MCG 11-14-25A	0.30[b]	1.38[a]	3.34	148[e]	0.185±0.007	0.097±0.001	−19.08	10.05	4.34	–
14	NGC 0524	0.27[b]	1.57[a]	3.50	253[a]	0.218±0.035	0.034±0.001	−21.85	10.67	4.55	0.325
15	NGC 0545	0.10[b]	2.16[a]	4.36	242[a]	0.462±0.059	0.239±0.001	−22.98	11.49	16.99	–
16	NGC 0584	0.30[b]	0.95[a]	3.53	207[a]	0.106±0.028	0.250±0.001	−21.38	10.53	7.06	–
17	NGC 0741	0.11[b]	2.46[a]	4.12	291[a]	0.090±0.037	0.128±0.001	−23.27	11.41	6.18	–
18	NGC 1016	0.11[b]	2.25[a]	2.10	294[a]	−0.026±0.035	0.066±0.001	−22.90	9.40	7.74	–
19	NGC 1052	0.22[b]	1.46[a]	3.45	208[a]	−0.773±0.001	0.265±0.001	−21.17	10.45	2.75	–
20	NGC 1700	0.07[b]	1.01[a]	3.64	235[a]	0.986±0.029	0.266±0.001	−21.95	10.75	12.12	–
21	NGC 2832	0.03[b]	2.52[a]	4.93	335[a]	−0.333±0.003	0.192±0.001	−23.76	12.35	9.08	–
22	NGC 3193	0.28[b]	1.38[a]	3.49	194[a]	0.317±0.001	0.161±0.001	−21.98	10.43	4.92	0.197
23	NGC 3379	0.18[b]	1.72[a]	3.67	207[a]	−0.028±0.001	0.098±0.001	−21.14	10.67	6.66	0.157
24	NGC 3551	0.14[b]	2.37[a]	5.44	268[a]	0.374±0.005	0.173±0.001	−23.55	12.66	9.43	–
25	NGC 3607	0.26[b]	1.77[a]	3.51	224[a]	−0.099±0.001	0.192±0.001	−19.88	10.58	4.61	0.228
26	NGC 3608	0.17[b]	1.31[a]	3.73	193[a]	−0.420±0.001	0.175±0.001	−21.12	10.67	5.71	0.043
27	NGC 3613	0.08[b]	1.65[a]	3.56	210[a]	−0.123±0.003	0.313±0.001	−21.59	10.57	2.92	0.191
28	NGC 3640	0.03[b]	1.47[a]	3.41	182[a]	−0.305±0.001	0.214±0.001	−21.96	10.30	3.41	0.320
29	NGC 3842	0.12[b]	2.48[a]	4.41	314[a]	−0.387±0.003	0.149±0.001	−23.18	11.77	5.59	–
30	NGC 4073	−0.08[b]	2.13[a]	4.56	278[a]	0.349±0.003	0.297±0.001	−23.50	11.81	5.16	–
31	NGC 4168	0.17[b]	2.26[a]	3.76	184[a]	0.804±0.002	0.155±0.001	−21.80	10.66	3.61	0.040
32	NGC 4261	0.00[b]	2.31[a]	3.96	309[a]	−1.372±0.001	0.256±0.001	−22.26	11.31	5.31	0.085
33	NGC 4278	0.10[b]	1.77[a]	3.16	238[a]	−0.280±0.001	0.148±0.001	−21.05	10.28	4.49	0.203
34	NGC 4365	0.09[b]	2.15[a]	4.06	256[a]	−1.181±0.001	0.238±0.001	−22.18	11.24	6.26	0.088
35	NGC 4371	0.27[c]	1.60[c]	3.24	–	0.512±0.061	0.257±0.002	−20.00	–	3.43	0.482
36	NGC 4374	0.13[b]	2.11[a]	3.79	282[a]	−0.401±0.001	0.183±0.002	−22.28	11.06	5.62	0.024

37	NGC 4382	0.01^{b}	1.69^{a}	4.04	179^{a}	0.852±0.001	0.212±0.001	−21.96	10.91	6.00	0.163
38	NGC 4406	-0.04^{b}	1.90^{a}	3.34	235^{a}	−0.763±0.001	0.180±0.001	−22.46	10.45	6.68	0.052
39	NGC 4458	0.17^{b}	0.80^{a}	3.51	103^{a}	0.395±0.003	0.138±0.001	−19.27	9.90	6.97	0.079
40	NGC 4472	0.01^{b}	2.25^{a}	3.56	291^{a}	−0.227±0.001	0.087±0.001	−22.93	10.85	3.01	0.077
41	NGC 4473	0.01^{b}	1.73^{a}	3.67	179^{a}	1.149±0.001	0.388±0.001	−21.16	10.54	4.28	0.250
42	NGC 4478	0.10^{b}	1.32^{a}	3.08	138^{a}	−0.449±0.002	0.181±0.001	−19.89	9.73	1.84	0.177
43	NGC 4486	0.27^{b}	2.65^{a}	3.53	332^{a}	−0.098±0.001	0.017±0.001	−22.71	10.94	2.14	–
44	NGC 4486B	-0.10^{b}	1.08^{a}	2.49	170^{a}	0.458±0.005	0.110±0.002	−17.98	9.32	2.10	0.021
45	NGC 4552	-0.02^{b}	1.60^{a}	2.89	253^{a}	−0.010±0.001	0.050±0.001	−21.65	10.06	4.43	0.049
46	NGC 4636	0.13^{b}	2.21^{a}	3.59	203^{a}	−0.018±0.001	0.026±0.001	−21.86	10.57	3.44	0.036
47	NGC 4649	0.17^{b}	2.34^{a}	3.62	336^{a}	−0.477±0.001	0.113±0.001	−22.51	11.04	3.23	0.127
48	NGC 4874	0.12^{b}	2.99^{a}	4.80	278^{a}	−0.058±0.003	0.074±0.001	−23.49	12.05	4.96	–
49	NGC 4889	0.03^{b}	2.84^{a}	4.11	401^{a}	−0.563±0.002	0.268±0.001	−23.73	11.68	3.41	–
50	NGC 5198	0.26^{b}	1.33^{a}	3.60	196^{a}	−0.249±0.003	0.130±0.001	−21.23	10.55	3.53	0.057
51	NGC 5322	0.15^{c}	2.02^{c}	3.64	–	−0.001±0.029	0.320±0.001	−21.41	–	6.11	0.067
52	NGC 5485	0.19^{c}	1.90^{c}	3.75	176^{e}	−0.599±0.450	0.068±0.010	−21.14	10.61	5.09	0.149
53	NGC 5557	0.07^{b}	1.82^{a}	3.99	254^{a}	−0.274±0.002	0.202±0.001	−22.62	11.17	5.33	0.045
54	NGC 5576	0.26^{b}	1.21^{a}	3.36	183^{a}	−0.642±0.001	0.258±0.001	−21.31	10.25	4.65	0.091
55	NGC 5813	0.06^{b}	1.89^{a}	4.72	239^{a}	0.042±0.001	0.095±0.001	−22.01	11.84	8.50	0.071
56	NGC 5982	0.05^{b}	1.80^{a}	3.81	240^{a}	−1.241±0.002	0.281±0.001	−21.97	10.94	4.92	–
57	NGC 6086	0.02^{b}	2.53^{a}	4.57	336^{a}	−0.562±0.005	0.268±0.001	−23.11	11.99	7.36	–
58	NGC 6166	0.12^{b}	3.17^{a}	4.40	310^{a}	−0.372±0.005	0.203±0.002	−23.80	11.75	2.75	–
59	NGC 6173	0.02^{b}	2.32^{a}	4.60	278^{a}	−0.334±0.004	0.332±0.001	−23.59	11.85	6.87	–
60	NGC 7578B	0.21^{b}	2.06^{a}	4.57	214^{a}	0.499±0.085	0.170±0.002	−23.41	11.60	16.47	–
61	NGC 7619	0.01^{b}	2.03^{a}	3.97	322^{a}	0.238±0.036	0.231±0.001	−22.94	11.35	6.25	–
62	NGC 7647	0.05^{b}	2.28^{a}	3.00	282^{a}	0.994±0.294	0.290±0.035	−23.97	10.27	15.58	–
63	NGC 7785	0.06^{b}	1.32^{a}	3.62	245^{a}	−1.708±0.040	0.388±0.001	−22.08	10.76	4.84	–

Notes: Column (1): Number; Col. (2): Galaxy Name; Cols. (3) and (4): The local slope of "Nuker Law" fits and "Cusp radius," ^{a} from Lauer et al. (2007a); ^{b} from Lauer et al. (2007b); ^{c} from Krajnović et al. (2013); ^{d} from Hyde et al. (2008). Col.(5): Effective radius from best Sérsic fits; Col. (6): Central velocity dispersion; ^{e} from the SDSS DR8 Spectroscopic catalog. Col. (7): Isophotal shape parameter a_4/a; Col.(8): Ellipticity; Col.(9): Absolute magnitude in the V-band; Col. (10): The dynamical mass; Col. (11): Sérsic index; Col. (12): Specific angular momentum parameter from Emsellem et al. (2011).

Table 2 "Power-law" Galaxy Parameters

No.	Galaxy	γ'	r_γ	$R_{\rm e}$	σ	a_4/a	ε	M_V	$\log\frac{M_{\rm dyn}}{M_\odot}$	n	$\lambda_{R_{\rm e}/2}$
			log(pc)	log(pc)	(km s^{-1})	(10^{-2})		(mag)			
(1)	(2)	(3)	(4)	(5)	(6)	(7)	(8)	(9)	(10)	(11)	(12)
1	IC 0875	1.12^{b}	1.01^{a}	4.27	–	0.679±0.006	0.394±0.001	−20.21	–	11.20	–
2	IC 2738	0.60^{b}	1.57^{a}	4.04	275^{a}	0.202±0.009	0.068±0.002	−22.18	11.29	5.84	–
3	J013431.5+131436.4	0.54^{d}	–	4.17	248^{e}	−0.214±0.309	0.524±0.024	−23.17	11.33	9.65	–
4	J082216.5+481519.1	0.94^{d}	–	5.90	351^{e}	−0.170±0.155	0.305±0.012	−21.26	13.36	15.00	–
5	J082646.7+495211.5	1.14^{d}	–	4.47	–	0.113±0.160	0.305±0.014	−22.10	–	4.83	–
6	J093124.4+574926.6	0.52^{d}	–	4.17	350^{e}	0.988±0.117	0.235±0.012	−22.95	11.62	2.20	–
7	J103344.2+043143.5	0.80^{d}	–	4.12	335^{e}	−0.258±0.117	0.414±0.010	−22.36	11.54	3.36	–
8	J111525.7+024033.9	0.76^{d}	–	4.34	379^{e}	−0.833±0.108	0.265±0.011	−23.40	11.86	3.21	–
9	J151741.7−004217.6	1.10^{d}	–	3.93	380^{e}	0.115±0.059	0.215±0.005	−21.67	11.46	3.10	–
10	J160239.1+022110.0	0.61^{d}	–	4.00	358^{e}	1.654±0.198	0.271±0.017	−22.91	11.47	3.08	–
11	J221414.3+131703.7	1.09^{d}	–	3.60	–	1.689±0.094	0.274±0.009	−21.85	–	2.18	–
12	MCG 08-27-18	0.89^{b}	1.07^{a}	3.18	89^{a}	−0.074±0.006	0.076±0.001	−20.03	9.45	3.41	–
13	NGC 0474	0.56^{b}	1.15^{a}	3.59	164^{a}	−0.212±0.043	0.122±0.001	−20.12	10.39	9.24	0.210
14	NGC 0596	0.54^{b}	0.63^{a}	3.51	152^{a}	0.034±0.029	0.069±0.001	−20.90	10.24	8.28	–
15	NGC 0936	0.52^{c}	0.87^{c}	3.50	–	0.145±0.025	0.108±0.001	−20.84	–	6.13	0.430
16	NGC 2549	0.67^{b}	0.51^{a}	3.25	143^{a}	1.938±0.003	0.447±0.001	−19.17	9.93	3.18	0.523
17	NGC 2592	0.92^{b}	0.82^{a}	3.24	265^{a}	0.579±0.003	0.158±0.001	−20.01	10.45	3.53	0.431
18	NGC 2685	0.73^{b}	0.84^{a}	3.23	94^{a}	3.180±0.004	0.533±0.002	−19.72	9.54	3.59	0.632
19	NGC 2778	0.83^{b}	0.67^{a}	3.31	162^{a}	0.721±0.004	0.208±0.001	−18.75	10.10	1.86	0.435
20	NGC 2859	0.76^{c}	0.77^{c}	3.18	–	1.109±0.035	0.188±0.001	−20.83	–	3.60	0.361
21	NGC 2872	1.01^{b}	1.06^{a}	3.65	285^{a}	−0.147±0.002	0.200±0.001	−21.62	10.93	4.15	–
22	NGC 2880	0.75^{c}	1.01^{c}	3.29	281^{e}	−0.215±0.035	0.210±0.001	−20.31	10.56	4.95	0.482
23	NGC 2950	0.82^{b}	0.58^{a}	3.27	182^{a}	0.819±0.002	0.242±0.001	−19.73	10.16	5.17	0.428

24	NGC 2962	0.80[c]	1.21[c]	3.77	–	1.509±0.076	0.280±0.001	−20.42	–	8.37	0.329
25	NGC 3156	1.78[c]	1.02[c]	3.85	–	−0.252±0.062	0.435±0.001	−19.36	–	8.62	0.559
26	NGC 3226	0.83[c]	0.57[c]	3.87	–	−0.267±0.048	0.162±0.001	−19.59	–	9.59	0.257
27	NGC 3245	0.74[c]	0.99[c]	3.63	850[e]	0.476±0.032	0.318±0.001	−20.62	11.86	8.60	0.592
28	NGC 3266	0.66[b]	0.85[a]	3.40	–	1.889±0.005	0.117±0.002	−20.11	–	7.15	–
29	NGC 3377	0.62[b]	0.36[a]	3.37	139[a]	0.446±0.001	0.343±0.006	−20.07	10.02	4.55	0.522
30	NGC 3384	0.71[b]	0.36[a]	4.22	148[a]	0.995±0.001	0.251±0.001	−19.93	10.93	14.90	0.397
31	NGC 3412	0.67[c]	0.73[c]	3.40	–	0.146±0.035	0.254±0.001	−19.96	–	11.29	0.403
32	NGC 3414	0.84[b]	0.81[a]	3.82	237[a]	1.746±0.002	0.216±0.001	−20.25	10.94	6.07	0.070
33	NGC 3458	0.59[c]	1.17[c]	3.18	–	−0.146±0.037	0.120±0.001	−19.86	–	8.41	0.250
34	NGC 3489	0.57[c]	0.72[c]	2.84	–	−0.238±0.043	0.250±0.002	−19.30	–	4.64	0.552
35	NGC 3595	0.76[b]	0.93[a]	3.39	–	−0.316±0.004	0.343±0.001	−20.96	–	2.87	0.301
36	NGC 3599	0.75[b]	0.65[a]	3.77	85[a]	0.264±0.003	0.115±0.001	−19.93	10.00	7.45	0.239
37	NGC 3605	0.60[b]	0.65[a]	2.52	92[a]	−0.734±0.037	0.261±0.001	−19.61	8.81	2.23	0.347
38	NGC 3610	0.76[b]	0.64[a]	3.28	162[a]	2.128±0.003	0.437±0.002	−20.96	10.07	3.96	0.539
39	NGC 3796	0.74[c]	1.04[c]	2.88	–	0.125±0.052	0.370±0.001	−18.66	–	10.39	0.119
40	NGC 3900	1.02[b]	1.16[a]	3.61	118[a]	0.294±0.003	0.233±0.002	−20.80	10.12	2.25	–
41	NGC 3945	0.57[b]	0.59[a]	3.37	174[a]	2.645±0.003	0.230±0.001	−20.25	10.22	5.03	0.561
42	NGC 4026	0.65[b]	0.48[a]	3.26	178[a]	4.249±0.003	0.368±0.002	−19.79	10.13	2.52	0.442
43	NGC 4121	0.85[b]	0.79[a]	2.73	86[a]	−0.085±0.005	0.242±0.001	−18.53	8.97	1.32	–
44	NGC 4128	0.75[b]	0.92[a]	3.48	203[a]	−0.498±0.042	0.370±0.001	−20.79	10.46	9.25	–
45	NGC 4143	0.61[b]	0.88[a]	3.09	214[a]	0.714±0.002	0.228±0.001	−19.68	10.12	2.62	0.398
46	NGC 4150	0.68[b]	0.85[a]	3.49	85[a]	0.084±0.002	0.209±0.002	−18.66	9.72	10.40	0.338
47	NGC 4203	0.74[c]	0.85[c]	2.98	–	0.655±0.028	0.082±0.001	−19.83	–	4.89	0.275
48	NGC 4262	0.76[c]	0.87[c]	2.81	–	0.228±0.025	0.099±0.001	−20.04	–	4.31	0.250
49	NGC 4267	0.71[c]	0.88[c]	2.92	–	0.769±0.024	0.073±0.001	−19.78	–	3.94	0.253
50	NGC 4281	0.56[c]	1.04[c]	4.20	–	0.774±0.041	0.463±0.001	−21.84	–	12.00	0.621
51	NGC 4283	0.80[c]	1.04[c]	2.75	–	−0.091±0.031	0.052±0.001	−18.72	–	3.39	0.151
52	NGC 4339	0.81[c]	0.87[c]	3.59	–	−0.020±0.033	0.051±0.001	−19.95	–	7.30	0.312
53	NGC 4340	0.68[c]	0.89[c]	3.94	–	0.558±0.131	0.192±0.003	−19.44	–	12.35	0.442
54	NGC 4342	0.55[c]	0.84[c]	3.23	219[e]	3.559±0.102	0.445±0.002	−18.13	10.28	8.00	0.306
55	NGC 4387	0.65[b]	0.54[a]	2.71	104[a]	−1.414±0.003	0.304±0.001	−19.25	9.11	2.35	0.317
56	NGC 4417	0.75[b]	0.94[a]	3.24	131[a]	1.868±0.002	0.345±0.001	−18.94	9.84	4.68	0.392
57	NGC 4429	1.07[c]	0.58[c]	4.33	–	−0.1344±0.044	0.442±0.001	−20.41	–	9.35	0.396
58	NGC 4434	0.64[b]	0.54[a]	3.00	120[a]	0.124±0.003	0.062±0.001	−19.19	9.52	3.91	0.199
59	NGC 4442	0.52[c]	0.72[c]	2.97	59[e]	−0.622±0.032	0.285±0.001	−19.04	8.88	4.90	0.338
60	NGC 4464	0.70[b]	0.54[a]	2.80	127[a]	0.714±0.003	0.280±0.001	−18.82	9.37	3.24	–
61	NGC 4467	0.94[b]	0.54[a]	2.91	68[a]	0.606±0.007	0.285±0.001	−17.51	8.94	4.00	–
62	NGC 4474	0.72[b]	0.72[a]	3.45	87[a]	2.271±0.004	0.267±0.001	−18.42	9.70	3.93	0.353
63	NGC 4483	0.88[c]	0.91[c]	3.38	92[e]	−0.245±0.056	0.262±0.001	−18.44	9.68	8.27	0.273
64	NGC 4486A	0.72[c]	0.95[c]	2.98	–	−0.046±0.072	0.244±0.005	−18.92	–	5.16	0.351
65	NGC 4489	0.64[c]	0.87[c]	4.41	62[e]	0.174±0.061	0.088±0.001	−18.64	10.37	9.39	0.117
66	NGC 4494	0.55[b]	0.54[a]	3.68	150[a]	0.032±0.001	0.148±0.001	−21.50	10.40	3.69	0.212
67	NGC 4503	0.65[b]	0.63[a]	4.28	111[a]	0.029±0.002	0.270±0.001	−19.57	10.74	7.69	0.470
68	NGC 4528	0.97[c]	0.88[c]	2.94	–	−0.615±0.059	0.169±0.002	−19.72	–	3.72	0.102
69	NGC 4550	0.57[c]	0.88[c]	2.59	–	2.086±0.086	0.582±0.001	−17.32	–	1.94	0.061
70	NGC 4551	0.69[b]	0.54[a]	3.12	108[a]	−0.456±0.002	0.260±0.001	−19.37	9.55	2.14	0.259
71	NGC 4564	0.81[b]	0.63[a]	3.36	157[a]	1.426±0.002	0.333±0.001	−20.26	10.12	4.50	0.536
72	NGC 4570	0.85[c]	0.92[c]	3.51	–	1.154±0.073	0.396±0.001	−21.26	–	6.48	0.498
73	NGC 4578	0.89[c]	0.90[c]	3.81	–	0.342±0.033	0.233±0.001	−21.01	–	7.66	0.544
74	NGC 4596	0.77[c]	0.90[c]	4.04	–	1.289±0.058	0.216±0.001	−21.42	–	7.31	0.280
75	NGC 4612	0.64[c]	0.91[c]	4.60	–	−0.207±0.041	0.192±0.001	−20.79	–	16.74	0.324
76	NGC 4621	0.85[b]	0.54[a]	3.43	225[a]	1.539±0.001	0.325±0.001	−21.74	10.50	6.06	0.291
77	NGC 4623	2.06[c]	0.93[c]	3.59	–	1.112±0.100	0.562±0.001	−19.80	–	5.02	0.564
78	NGC 4638	0.77[c]	0.93[c]	3.04	–	3.801±0.172	0.538±0.002	−20.03	–	3.41	0.715
79	NGC 4660	0.91[b]	0.54[a]	2.99	188[a]	1.100±0.002	0.345±0.001	−20.13	9.90	3.90	0.475
80	NGC 4754	0.60[c]	0.04[c]	3.70	–	−0.038±0.032	0.182±0.001	−20.84	–	8.79	0.418
81	NGC 5173	0.52[c]	1.27[c]	3.48	99[e]	0.140±0.036	0.121±0.001	−20.09	9.84	9.26	0.106
82	NGC 5273	1.66[c]	0.89[c]	3.85	90[e]	0.130±0.052	0.135±0.001	−19.45	10.13	10.00	0.482
83	NGC 5308	0.96[b]	0.90[a]	3.51	211[a]	3.143±0.004	0.467±0.001	−21.26	10.53	3.05	0.510
84	NGC 5370	0.67[b]	1.04[a]	3.54	133[a]	3.403±0.010	0.294±0.002	−20.60	10.15	4.38	–
85	NGC 5831	0.55[b]	0.85[a]	3.67	164[a]	0.305±0.002	0.272±0.001	−21.00	10.47	5.11	0.065

86	NGC 5838	0.93[b]	1.03[a]	3.52	266[a]	−0.057±0.002	0.167±0.002	−20.51	10.74	4.73	0.460
87	NGC 5845	0.52[b]	1.14[a]	2.64	234[a]	−0.497±0.002	0.255±0.001	−19.98	9.74	2.95	0.358
88	NGC 5854	1.01[c]	0.39[c]	3.76	–	−0.471±0.091	0.370±0.001	−20.41	–	9.08	0.515
89	NGC 6278	0.67[b]	0.99[a]	3.66	150[a]	0.653±0.003	0.233±0.001	−20.81	10.38	6.26	0.411
90	NGC 6340	0.64[b]	0.91[a]	3.56	144[a]	−0.174±0.002	0.036±0.001	−19.46	10.24	15.97	–
91	NGC 7280	0.87[c]	1.06[c]	4.17	–	−0.485±0.062	0.329±0.001	−20.37	–	9.98	0.503
92	NGC 7332	0.80[b]	0.67[a]	3.20	124[a]	2.196±0.178	0.487±0.002	−19.62	9.75	8.70	0.338
93	NGC 7743	0.57[b]	1.03[a]	3.60	84[a]	1.058±0.103	0.293±0.001	−20.18	9.82	16.97	–
94	UGC 4551	0.51[b]	0.82[a]	2.89	167[a]	−0.156±0.002	0.145±0.001	−19.78	9.70	3.10	–
95	UGC 4587	0.81[b]	1.05[a]	3.81	–	−0.378±0.006	0.320±0.001	−20.77	–	4.77	–
96	UGC 6062	0.82[b]	1.01[a]	3.26	142[e]	0.339±0.005	0.250±0.001	−20.34	9.93	3.53	–
97	VCC 1199	0.90[b]	0.54[a]	3.97	55[e]	0.484±0.015	0.025±0.001	−15.58	9.82	10.00	–
98	VCC 1440	0.89[b]	0.54[a]	2.41	–	0.140±0.008	0.129±0.002	−17.24	–	3.30	–
99	VCC 1545	0.51[b]	0.54[a]	3.30	51[e]	−0.215±0.012	0.144±0.004	−17.49	9.08	2.89	–
100	VCC 1627	0.69[b]	0.54[a]	1.93	–	0.097±0.009	0.089±0.002	−16.42	–	1.78	–

Notes: See the notes in Table 1 for each column.

Table 3 "Intermediate" Galaxy Parameters

No.	Galaxy	γ'	r_γ	$R_{\rm e}$	σ	a_4/a	ε	M_V	$\log\frac{M_{\rm dyn}}{M_\odot}$	n	$\lambda_{R_{\rm e}/2}$
			log(pc)	log(pc)	(km s^{-1})	(10^{-2})		(mag)			
(1)	(2)	(3)	(4)	(5)	(6)	(7)	(8)	(9)	(10)	(11)	(12)
1	J091944.2+562201.1	0.32[d]	–	4.97	327[e]	−1.982±0.134	0.198±0.020	−23.84	12.37	6.46	–
2	J112842.0+043221.7	0.47[d]	–	4.01	360[e]	−1.068±0.194	0.249±0.021	−22.86	11.49	3.09	–
3	J120011.1+680924.8	0.33[d]	–	4.69	380[e]	1.249±0.078	0.310±0.009	−23.95	12.22	4.66	–
4	J133724.7+033656.5	0.37[d]	–	4.83	414[e]	−1.755±0.079	0.167±0.008	−22.50	12.43	10.05	–
5	J135602.4+021044.6	0.40[d]	–	4.26	352[e]	−1.807±0.109	0.272±0.010	−23.89	11.72	4.89	–
6	J162332.4+450032.0	0.35[d]	–	4.65	356[e]	0.142±0.068	0.202±0.007	−23.14	12.12	4.82	–
7	NGC 2841	0.34[b]	1.09[a]	3.76	206[a]	1.778±0.001	0.286±0.001	−20.57	10.75	12.98	–
8	NGC 3998	0.49[c]	0.83[c]	2.71	–	0.424±0.066	0.147±0.002	−19.58	–	2.17	0.342
9	NGC 4239	0.46[b]	1.06[a]	3.03	62[a]	1.051±0.004	0.420±0.001	−18.50	8.98	2.56	–
10	NGC 4270	0.44[c]	1.62[c]	3.66	–	−0.527±0.048	0.420±0.001	−20.79	–	5.75	0.294
11	NGC 4350	0.47[c]	1.57[c]	3.24	–	2.411±0.132	0.415±0.001	−20.44	–	5.00	0.480
12	NGC 4377	0.41[c]	1.17[c]	3.75	–	0.587±0.035	0.157±0.001	−19.90	–	15.19	0.338
13	NGC 4379	0.46[c]	1.02[c]	3.18	–	0.442±0.031	0.182±0.001	−19.47	–	5.04	0.300
14	NGC 4452	0.39[c]	2.37[c]	2.38	45[e]	2.301±0.287	0.667±0.008	−15.52	8.05	1.22	0.648
15	NGC 4476	0.34[c]	2.32[c]	3.25	49[e]	2.432±0.175	0.426±0.003	−20.27	9.01	2.92	0.266
16	NGC 4477	0.38[c]	1.38[c]	3.43	–	2.203±0.069	0.218±0.001	−21.05	–	4.02	0.221
17	NGC 4482	0.49[b]	2.05[a]	3.59	26[a]	−0.260±0.005	0.324±0.001	−18.87	8.79	2.40	–
18	NGC 4733	0.35[c]	1.90[c]	3.55	–	1.240±0.066	0.224±0.001	−18.70	–	4.60	0.076
19	NGC 4762	0.40[c]	1.42[c]	3.13	–	2.335±0.056	0.513±0.002	−20.20	–	7.10	0.724
20	NGC 5422	0.45[c]	1.30[c]	3.97	–	2.186±0.076	0.385±0.002	−20.19	–	12.22	0.501
21	NGC 5475	0.40[c]	1.49[c]	3.76	102[e]	0.874±0.090	0.450±0.001	−19.78	10.15	9.88	0.638

Notes: See the notes in Table 1 for each column.

4 RESULTS AND DISCUSSION

4.1 The Relations between a_4/a and Properties of the Central Region of ETGs

In this subsection, we re-visit the relations between the isophotal shape described by parameter a_4/a and the photometric properties of the central regions of ETGs.

Figure 1 shows the distributions of a_4/a for "core" and "power-law" ETGs. It is clear from the histograms shown in Figure 1 that the distribution of a_4/a for "core" and "power-law" ETGs is not significantly separated, i.e. the a_4/a distribution of a large fraction of "core" and "power-law" ETGs overlap. The fractions of boxy and disky galaxies are 59% (37/63) and 41% (26/63) for "core" ETGs, and the median value of a_4/a is -0.26×10^{-3}. For the 100 "power-law" ETGs, the

fractions of boxy and disky galaxies are ∼35% (35/100) and 65% (65/100), respectively, and the median of a_4/a is 1.88×10^{-3}. It suggests that "core" galaxies are not necessarily boxy, and only two-thirds of "power-law" galaxies show disky isophotes. However, the galaxies with highest a_4/a are "power-law" galaxies.

The left panel of Figure 2 shows a_4/a as a function of γ' that describes the slope of the central surface brightness profile of ETGs (see Lauer et al. 2007b). The two dotted vertical lines in Figure 2 divide the sample of ETG into "core," "intermediate" and "power-law" galaxies, while the disky and boxy ETGs are located above and below the horizontal dotted line respectively. Although there is a trend that the values of a_4/a increase as γ' increases, the scatter shown in Figure 2 is quite large, i.e. the correlation between a_4/a and γ' is weak. The Spearman rank-order correlation coefficient between a_4/a and γ' is $r_s = 0.24$ and the probability that no correlation exists between these two parameters is 1.12×10^{-3}. Apart from the slope of the central light profiles γ', the values of r_γ characterize the physical scale of the core regions of ETGs ("cusp radius," Lauer et al. 2007a). Lauer et al. (2007a) claimed that the core size r_γ is tightly correlated with the galaxy luminosity L and the black hole mass $M_\bullet$. However, from the right panel of Figure 2 that shows a_4/a is a function of r_γ, there is no correlation found between a_4/a and r_γ for "core" ETGs.

Note that Bender et al. (1989) pointed out that a_4/a might be influenced by the projection effect, but such effect could only lead to a change in its absolute value, not the sign of a_4/a. Thus the classification of boxy and disky ETGs reflects the intrinsic isophotal property of ETGs. Therefore the statistical results shown above do not support the statement that there is a close relation between isophotal shape and their central light profile for ETGs.

4.2 The Relations between a_4/a and the Global Properties of ETGs

In this subsection, we investigate relations between the isophotal shape and other global properties of "core" and "power-law" ETGs. The left panel of Figure 3 shows a_4/a as a function of the V-band luminosity (M_V). It can be seen from the left panel of Figure 3 that there is a weak correlation between a_4/a and M_V for the whole sample of ETGs, indicating that boxy (disky) ETGs tend to be bright (faint). Faber et al. (1997) pointed out that luminous galaxies with $M_V < -22$ mag have shallow "core" inner profiles, faint galaxies with $M_V > -20.5$ mag show steep "power-law" inner profiles, and for those with $-22 < M_V < -20.5$, "core" and "power-law" galaxies coexist. Therefore, it is interesting to visit the fractions of boxy and disky galaxies in these luminosity intervals. The fraction of boxy (disky) galaxies is ∼32% (68%) for faint ETGs with $M_V > -20.5$ mag, but is ∼58% (42%) for the most luminous ETGs with $M_V < -22$ mag. For ETGs in the luminosity interval of $-22 < M_V < -20.5$, the fractions of boxy and disky galaxies are similar (∼46% and 54%, respectively). These results are consistent with Hao et al. (2006). On the other hand, the fraction of "core" ("power-law") is ∼7% (79%) for faint ETGs with $M_V > -20.5$ mag, but is ∼74% (14%) for the most luminous ETGs with $M_V < -22$ mag. In the luminosity interval of $-22 < M_V < -20.5$, the fractions are comparable for "core" and "power-law" ETGs (∼41% and 53%, respectively). Thus we confirm the conclusion of Faber et al. (1997). In the right panel of Figure 3, we show the isophotal shape parameter a_4/a as a function of the dynamical mass. Similar to the left panel of Figure 3, there is a tendency that a_4/a decreases as ETGs become more massive and "core" ETGs become dominated by massive ETGs with dynamical mass larger than $10^{11} M_\odot$. Therefore, the bimodal classification based on the central light profile ("core" and "power-law") is more tightly correlated with galaxy luminosity and dynamical mass than that based on isophotal shape (boxy and disky).

As is well known, the Sérsic law is widely used to model the surface brightness profiles of ETGs and the best fitting value of the Sérsic index n could be used to describe the structures of galaxies. Based on photometric analysis for a sample of ETGs in the Virgo cluster, Kormendy (2009) claimed that giant ETGs characterized by $n > 4$ tend to rotate slowly, be less flattened (ellipticity ∼0.15) and

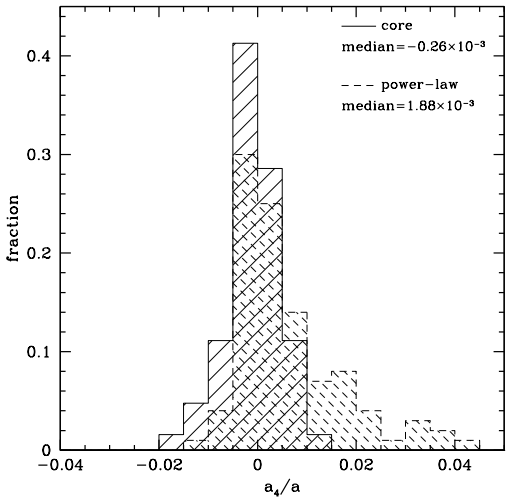

Fig. 1 Histograms of the parameter related to isophotal shape a_4/a for "core" (*solid line*) and "power-law" (*dashed line*) ETGs. The median values are indicated in the top right.

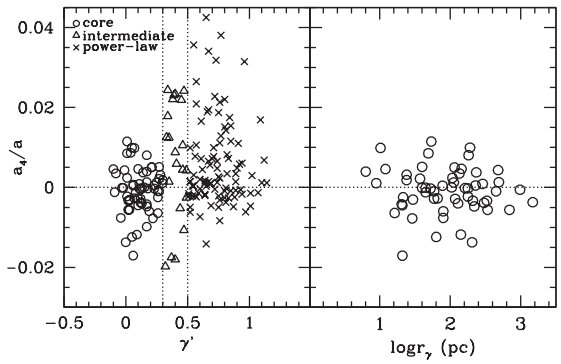

Fig. 2 The parameter a_4/a, that is related to the isophotal shape, as a function of (a) central surface brightness profile slope γ' (*left panel*) and (b) "cusp radius" r_γ for "core" galaxies (*right panel*). The horizontal dotted lines show the classification of disky ($a_4/a > 0$) and boxy ($a_4/a < 0$) isophotal shape, while the vertical dotted lines in the left panel show the separation of "core" ($\gamma' < 0.3$, circles), "power-law" ($\gamma' > 0.5$, crosses) and "intermediate" ETGs ($0.3 < \gamma' < 0.5$, triangles).

have boxy isophotes as well as being "core" in their center. To test whether this argument applies to our sample of ETGs, we plot a_4/a as a function of the Sérsic index n in Figure 4. It shows that there is no correlation between a_4/a and the Sérsic index n and the Sérsic index n is smaller than 4 for quite a few ETGs with "core" or boxy isophotes, which indicates that the central and isophotal properties of ETGs are not directly related to the Sérsic index n.

Moreover, the ATLAS^{3D} group (e.g. Cappellari et al. 2011) claimed that both isophotal shape and central light profile of ETGs are secondary indicators of the galaxy's kinematic structure. They strongly suggest using the specific angular momentum parameter λ_R as a discriminator of the bi-modal distribution of ETGs, i.e. separating fast from slow rotators. It is interesting to investigate relations among isophotal shapes, central light profiles and the kinematic properties as parametrized

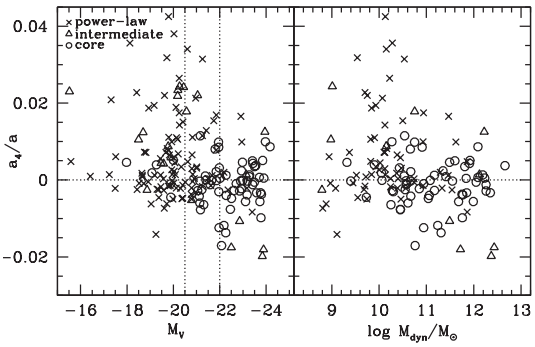

Fig. 3 Isophotal shape parameter a_4/a versus the V-band absolute magnitude M_V (*left panel*) and the dynamical mass (*right panel*). Circles represent "core" galaxies, triangles are "intermediate" galaxies and crosses show "power-law" galaxies. The horizontal dotted line is the separation of disky ($a_4/a > 0$) and boxy ($a_4/a < 0$) ETGs. The vertical dotted lines in the left panel indicate the less luminous galaxies with $M_V > -20.5$, more luminous galaxies with $M_V < -22$ and ETGs in the interval of $-22 < M_V < -20.5$ reported by Lauer et al. (2007b).

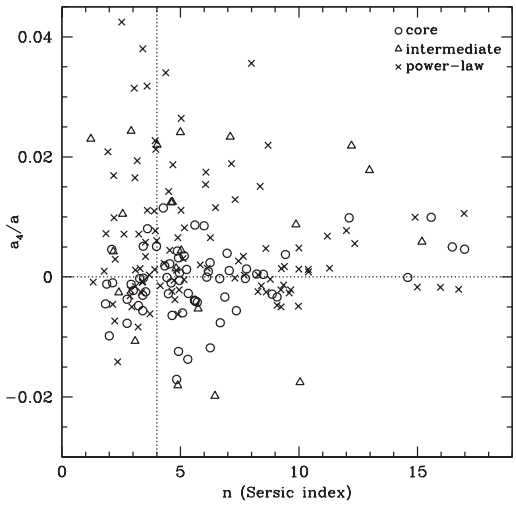

Fig. 4 Isophotal shape parameter a_4/a versus Sérsic index n. Circles represent "core" galaxies, triangles are "intermediate" galaxies and crosses show "power-law" galaxies. The horizontal dotted line is the separation of disky ($a_4/a > 0$) and boxy ($a_4/a < 0$) galaxies. The vertical dotted line indicates ETGs with $n = 4$ following Kormendy (2009).

by $\lambda_{R_e/2}$, which is the λ_R measured within half of the effective radius R_e. For our sample of ETGs, the specific angular momentum $\lambda_{R_e/2}$ is available for 111 objects from ATLAS^{3D}. The sample size is 1.8 times larger that of Lauer (2012) who only compared the central light profile to $\lambda_{R_e/2}$.

Figure 5 shows how a_4/a varies with $\lambda_{R_e/2}$ for "core" and "power-law" ETGs. The dotted vertical line represents the $\lambda_{R_e/2} = 0.25$ line dividing slow and fast rotators as suggested by Lauer (2012), while the horizontal dotted line divides boxy and disky galaxies. It can be clearly seen that there is a trend that a_4/a increases as $\lambda_{R_e/2}$ increases and the ETGs with highest a_4/a are fast

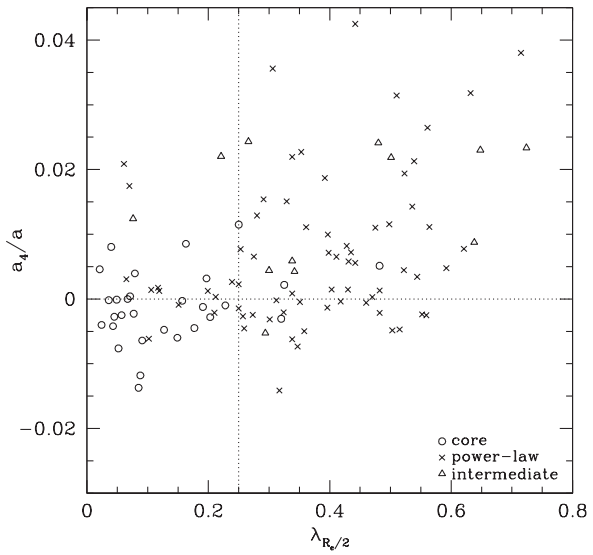

Fig. 5 Isophotal shape parameter a_4/a as a function of specific angular momentum $\lambda_{R_{\rm e}/2}$. The circles show "core" galaxies, triangles are "intermediate" galaxies and crosses show "power-law" galaxies. The horizontal dotted line separates disky ($a_4/a > 0$) and boxy ($a_4/a < 0$) galaxies. The vertical dotted line shows the discriminator of $\lambda_{R_{\rm e}/2} = 0.25$ between slow and fast rotators.

rotators. However, we can also see that such a trend is only apparent for power-law ETGs. We note that a_4/a and $\lambda_{R_{\rm e}/2}$ are both affected by inclination effects. However, inclination does not change the classification by considering isophotal shape or $\lambda_{R_{\rm e}/2}$ (Bender et al. 1989; Krajnović et al. 2013), so number statistics are more meaningful than the trend. The fraction of disky (boxy) galaxies is ∼70% (30%) for fast rotators ($\lambda_{R_{\rm e}/2} > 0.25$), but is ∼44% (56%) for slow rotators ($\lambda_{R_{\rm e}/2} < 0.25$). Emsellem et al. (2011) already investigated the relation between isophotal shape parameter a_4/a and kinematics of ETGs as characterized by $\lambda^N_{R\,{\rm e}} = \lambda_{R_{\rm e}}/\sqrt{\epsilon}$, and concluded that there is no simple correlation between these two parameters. Note that $\lambda^N_{R\,{\rm e}}$ has been corrected for the inclination effects and $\lambda^N_{R\,{\rm e}} = 0.31$ was used as a separator of slow and fast rotators by Emsellem et al. (2011). We also examined the relation between a_4/a and $\lambda^N_{R\,{\rm e}}$ based on our sample of ETGs, and found a similar result to Emsellem et al. (2011). Interestingly the fractions of disky/boxy galaxies in fast/slow rotators, classified by $\lambda^N_{R\,{\rm e}} = 0.31$, are similar to those classified by $\lambda_{R_{\rm e}/2} = 0.25$. Therefore, a possible physical connection exists between a_4/a and the kinematic properties of ETGs if the characteristic angular momentum parameter is influenced by the projection effect.

The ATLAS$^{\rm 3D}$ group (e.g. Krajnović et al. 2013) and Lauer (2012) both found that λ_R is correlated with the ellipticity ϵ, and the distribution of "core" and "power-law"galaxies can be well separated in the λ-ϵ diagram. It is interesting to study the relations between the isophotal shapes, ellipticity and nuclear profiles of galaxies.

Figure 6 shows a_4/a as a function of ϵ for "core" and "power-law" ETGs. It shows that there is a weak correlation between a_4/a and the ellipticity ϵ for "power-law" ETGs, but there is no correlation between these two parameters for "core" ETGs. From Figure 6, we note that the most distorted disky galaxies have the largest ellipticity, which agrees with what was found by Hao et al. (2006). In that work, this was explained as a consequence of a biased viewing angle. However, as shown in Figures 1 and 5, the ETGs with the largest a_4/a are also "power-law" and fast rotators. Hence, orientation cannot account for the high value of a_4/a, which may be caused by some physical pro-

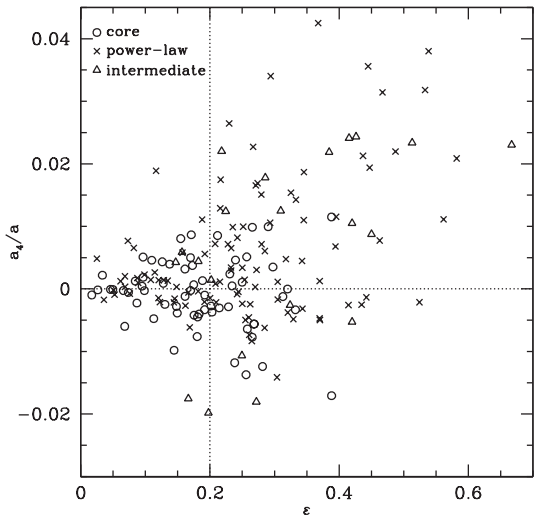

Fig. 6 Isophotal shape parameter a_4/a as a function of ellipticity ϵ. The circles show "core" galaxies, triangles are "intermediate" galaxies and crosses denote "power-law" galaxies. The horizontal dotted line divides disky ($a_4/a > 0$) and boxy ($a_4/a < 0$) galaxies. The vertical dotted line shows galaxies with an ellipticity separator of $\epsilon = 0.2$.

cesses. In particular, for those 111 ETGs that have $\lambda_{R_e/2}$ measurements available from ATLAS^{3D}, the Spearman rank-order correlation coefficients and the probabilities that no correlation exists for $\lambda_{R_e/2}$ versus ϵ and a_4/a versus ϵ are $r_s = 0.55, 0.38$ and Prob=3.96×10^{-10}, 3.61×10^{-5}, respectively. These values indicate that the correlation between kinematic properties and ellipticity is tighter than that between isophotal shape and ellipticity.

5 SUMMARY

In this paper, we study relations among isophotal shapes, central light profiles and kinematic properties of ETGs based on a compiled sample of 184 objects observed with both *HST* and SDSS DR8. Our main results are summarized as follows:

(1) There are no obvious relations between isophotal parameter a_4/a, the central light profile slope γ' and the central "cusp radius" r_γ. About 41% of "core" ETGs have disky isophotes, and 35% of "power-law" ETGs are boxy.
(2) Our statistical results show that there are only weak correlations between a_4/a and the galaxy luminosity M_V, and between a_4/a and the dynamical mass. Nuclear profiles correlate more tightly with M_V and dynamical mass. In addition, there is no correlation between a_4/a and the Sérsic index n.
(3) There are similar correlations between a_4/a and ellipticity and between a_4/a and the specific angular momentum $\lambda_{R_e/2}$, i.e. a_4/a is correlated with ellipticity and $\lambda_{R_e/2}$ for "power-law" ETGs, but no such relations exist for "core" ETGs. Quite a large fraction of fast rotator ETGs (70%) have disky isophotes, but the slowly rotating ETGs (56%) tend to be boxy. The disky galaxies with highest a_4/a are fast rotators and "power-law" ETGs.

Our statistical results support the statement by the ATLAS^{3D} group that the isophotal shape (a_4/a) of ETGs has no simple relation with both global and central properties of ETGs, but there

seems to be a correlation between a_4/a and the kinematic property for "power-law" ETGs. Galaxy formation is a very complicated process, as shown by both observations and simulations, which can lead to different morphologies, isophotal shapes, central light profiles, kinematic and other global physical properties. There indeed exist some trends among various physical parameters, but simple bimodal classifications may be too simplistic. As a caveat, our sample is compiled in a somewhat complicated way, so the numbers quoted in this paper may suffer from some selection effects.

Acknowledgements We thank Drs. Shude Mao and C. G. Shu for advice and helpful discussions. We also thank the anonymous referee for constructive comments. This project is supported by the National Natural Science Foundation of China (Grant Nos. 10973011, 10833006 and 11003015). The project was sponsored by SRF for ROCS, SEM. Funding for the creation and distribution of the SDSS Archive has been provided by the Alfred P. Sloan Foundation, the Participating Institutions, the National Aeronautics and Space Administration, the National Science Foundation, the U.S. Department of Energy, the Japanese Monbukagakusho, and the Max Planck Society. The SDSS-III website is *http://www.sdss3.org/*. The SDSS is managed by the Astrophysical Research Consortium (ARC) for the Participating Institutions. The Participating Institutions are the University of Chicago, Fermilab, the Institute for Advanced Study, the Japan Participation Group, Johns Hopkins University, the Korean Scientist Group, Los Alamos National Laboratory, the Max Planck Institute for Astronomy (MPIA), the Max Planck Institute for Astrophysics (MPA), New Mexico State University, University of Pittsburgh, Princeton University, the United States Naval Observatory, and the University of Washington.

References

Bender, R., Doebereiner, S., & Moellenhoff, C. 1988, A&AS, 74, 385
Bender, R., Surma, P., Doebereiner, S., Moellenhoff, C., & Madejsky, R. 1989, A&A, 217, 35
Bertin, E., & Arnouts, S. 1996, A&AS, 117, 393
Blanton, M. R., & Roweis, S. 2007, AJ, 133, 734
Cappellari, M., Emsellem, E., Bacon, R., et al. 2007, MNRAS, 379, 418
Cappellari, M., Emsellem, E., Krajnović, D., et al. 2011, MNRAS, 416, 1680
Crane, P., Stiavelli, M., King, I. R., et al. 1993, AJ, 106, 1371
de Zeeuw, P. T., Bureau, M., Emsellem, E., et al. 2002, MNRAS, 329, 513
Emsellem, E., Cappellari, M., Krajnović, D., et al. 2007, MNRAS, 379, 401
Emsellem, E., Cappellari, M., Krajnović, D., et al. 2011, MNRAS, 414, 888
Faber, S. M., Tremaine, S., Ajhar, E. A., et al. 1997, AJ, 114, 1771
Ferrarese, L., van den Bosch, F. C., Ford, H. C., Jaffe, W., & O'Connell, R. W. 1994, AJ, 108, 1598
Hao, C. N., Mao, S., Deng, Z. G., Xia, X. Y., & Wu, H. 2006, MNRAS, 370, 1339
He, Y. Q., Xia, X. Y., Hao, C. N., et al. 2013, ApJ, 773, 37
Hopkins, P. F., Cox, T. J., Dutta, S. N., et al. 2009a, ApJS, 181, 135
Hopkins, P. F., Lauer, T. R., Cox, T. J., Hernquist, L., & Kormendy, J. 2009b, ApJS, 181, 486
Hyde, J. B., Bernardi, M., Sheth, R. K., & Nichol, R. C. 2008, MNRAS, 391, 1559
Khochfar, S., & Burkert, A. 2005, MNRAS, 359, 1379
Kormendy, J. 2009, in Astronomical Society of the Pacific Conference Series, 419, Galaxy Evolution: Emerging Insights and Future Challenges, eds. S. Jogee, I. Marinova, L. Hao, & G. A. Blanc, 87
Kormendy, J., Fisher, D. B., Cornell, M. E., & Bender, R. 2009, ApJS, 182, 216
Krajnović, D., Emsellem, E., Cappellari, M., et al. 2011, MNRAS, 414, 2923
Krajnović, D., Karick, A. M., Davies, R. L., et al. 2013, MNRAS, 433, 2812
Laine, S., van der Marel, R. P., Lauer, T. R., et al. 2003, AJ, 125, 478
Lauer, T. R. 1985, MNRAS, 216, 429
Lauer, T. R. 2012, ApJ, 759, 64

Lauer, T. R., Ajhar, E. A., Byun, Y.-I., et al. 1995, AJ, 110, 2622
Lauer, T. R., Faber, S. M., Gebhardt, K., et al. 2005, AJ, 129, 2138
Lauer, T. R., Faber, S. M., Richstone, D., et al. 2007a, ApJ, 662, 808
Lauer, T. R., Gebhardt, K., Faber, S. M., et al. 2007b, ApJ, 664, 226
Liu, F. S., Xia, X. Y., Mao, S., Wu, H., & Deng, Z. G. 2008, MNRAS, 385, 23
Lupton, R., Gunn, J. E., Ivezić, Z., Knapp, G. R., & Kent, S. 2001, in Astronomical Society of the Pacific Conference Series, 238, Astronomical Data Analysis Software and Systems X, eds. F. R. Harnden, Jr., F. A. Primini, & H. E. Payne, 269
Naab, T., & Burkert, A. 2003, ApJ, 597, 893
Naab, T., & Trujillo, I. 2006, MNRAS, 369, 625
Peng, C. Y., Ho, L. C., Impey, C. D., & Rix, H.-W. 2002, AJ, 124, 266
Quillen, A. C., Bower, G. A., & Stritzinger, M. 2000, ApJS, 128, 85
Ravindranath, S., Ho, L. C., Peng, C. Y., Filippenko, A. V., & Sargent, W. L. W. 2001, AJ, 122, 653
Rest, A., van den Bosch, F. C., Jaffe, W., et al. 2001, AJ, 121, 2431
Sersic, J. L. 1968, Atlas de galaxias australes, Cordoba, Argentina: Observatorio Astronomico, 1968
Smith, J. A., Tucker, D. L., Kent, S., et al. 2002, AJ, 123, 2121
von der Linden, A., Best, P. N., Kauffmann, G., & White, S. D. M. 2007, MNRAS, 379, 867